Micro arch-bridge structured surface fabricated by kirigami-on-elastomer approach for liquid-dependent iso/anisotropic wetting

Atsushi Takei, Mayuko Murano, Marie Tani, Hiroyuki Fujita, and Ko Okumura

Citation: Appl. Phys. Lett. **110**, 161602 (2017); doi: 10.1063/1.4981255
View online: http://dx.doi.org/10.1063/1.4981255
View Table of Contents: http://aip.scitation.org/toc/apl/110/16
Published by the American Institute of Physics

Micro arch-bridge structured surface fabricated by kirigami-on-elastomer approach for liquid-dependent iso/anisotropic wetting

Atsushi Takei,[1,a)] Mayuko Murano,[2] Marie Tani,[3] Hiroyuki Fujita,[4] and Ko Okumura[1,2,3,a)]
[1]*Center for Soft Matter Physics, Ochanomizu University, 2-1-1 Otsuka, Bunkyo, Tokyo 112-8610, Japan*
[2]*Department of Physics, The Division of Advanced Sciences, Graduate School of Humanities of Sciences, Ochanomizu University, 2-1-1 Otsuka, Bunkyo, Tokyo 112-8610, Japan*
[3]*Faculty of Core Research, Ochanomizu University, 2-1-1 Otsuka, Bunkyo, Tokyo 112-8610, Japan*
[4]*Institute of Industrial Science, The University of Tokyo, 4-6-1 Komaba, Meguro, Tokyo 153-8505, Japan*

(Received 2 September 2016; accepted 6 April 2017; published online 19 April 2017)

Thin-film/elastomer bilayer systems have been studied for the fabrication of micro-structured surfaces. Here, we report a fabrication technique for three-dimensional microstructures by using thin ribbons partially attached to an elastomer substrate. This technique is an easy-to-use version of the conventional kirigami-on-elastomer approach. Parts of thin ribbons not attached to the elastomer substrate buckle under a fixed strain and form arch bridges with hollow spaces between the buckled ribbons and the elastomer substrate. We experimentally study the formation of the arch-bridge structure by changing applied strains to provide physical insights and find that the arch-bridge structure is useful as a functional surface. Although the arch-bridge structure was made with one-micron-thick ribbons, the structure is significantly robust. Different from the conventional structured surfaces made of micro-pillars, the micro arch-bridge structure exhibits an isotropic or an anisotropic wetting property depending on a liquid placed on the substrate. *Published by AIP Publishing.*
[http://dx.doi.org/10.1063/1.4981255]

Thin-film/elastomer bilayer systems have been studied for the fabrication of structured surfaces. Particularly, for micron-thick thin films, the representative length scale of patterns on the surface of a bilayer system becomes comparable to the film thickness, and such micro-patterns have been used as functional surfaces in applications such as hydrophobic surfaces,[1–3] optical devices,[4–7] smart adhesion,[8] and cell culture templates.[9–13] Ongoing efforts to study bilayer systems are partially motivated by possible applications for functional surfaces.

Another promising approach to achieve structured surfaces obtained from thin films is the kirigami-approach ("kiri" and "gami" stand for cut and paper in Japanese, respectively). By using a sheet with many cracks, the sheet deforms out-of-plane deformation under stretch and exhibits high stretchability. Exploiting the stretchability and non-planar structure, many applications such as stretchable graphenes,[14] stretchable lithium-ion batteries,[15] and integrated solar tracking systems[16] have been demonstrated by using kirigami sheets. Recently, besides such applications, the morphology and mechanical properties of kirigami[17,18] have been actively studied.

Inspired by ongoing studies on thin-film/elastomer bilayer systems and kirigami applications, Rogers *et al.*[19,20] reported a micro-fabrication technique for complex three-dimensional structures using thin films partially attached to an elastomer substrate (we call this and similar techniques the kirigami-on-elastomer approach). By applying compression to bilayer systems prepared with this method, various three-dimensional structures (e.g., table, flower, and helix) were achieved. In their work, due to the lack of technology for partially attaching thin films directly on an elastomer substrate in a desired shape, the thin film was patterned on a SiO_2 layer in the desired shape and then transferred onto the elastomer surface. The fabrication of high-aspect-ratio thin-film structures such as arch bridges is a still challenging problem in lithography-based micromachining, and the kirigami-on-elastomer approach is one of the promising methods. However, the transfer process requires multiple steps and fine tuning of the adhesive energy between the layers, which makes their kirigami-on-elastomer approach complicated. Because of this difficulty, their kirigami-on-elastomer approach, although a smart method, has been significantly limited in terms of applications.

Here, we present a variant of kirigami-on-elastomer approach using the chemical vapor deposition (CVD) process for attaching a thin film to an elastomer substrate. By virtue of technology for surface micromachining, we can pattern films in desired shapes and attach them on designed areas. With our proposed method, the transfer process is not required. As an example, in this study, thin film ribbons were partially attached to an elastomer substrate, and micro arch-bridge structures with hollow spaces were achieved by compressing the bilayer system as shown in Figure 1. The relationship between the applied strain and the geometry of the arch-bridge structure was studied experimentally, which leads to physical interpretations. Furthermore, we found that the hollow spaces allow the micro arch-bridge textured surface to exhibit a tunable liquid-dependent iso/anisotropic wetting property. The present study thereby proposes a promising method for bilayer systems to achieve functional surfaces.

The arch-bridge structure was fabricated as follows (Figure 2): the proposed method simplifies the fabrication process and broadens the potential of the kirigami-on-elastomer approach. We used an organic membrane, Parylene

[a)]Authors to whom correspondence should be addressed. Electronic addresses: takei.atsushi@ocha.ac.jp and okumura.ko@ocha.ac.jp

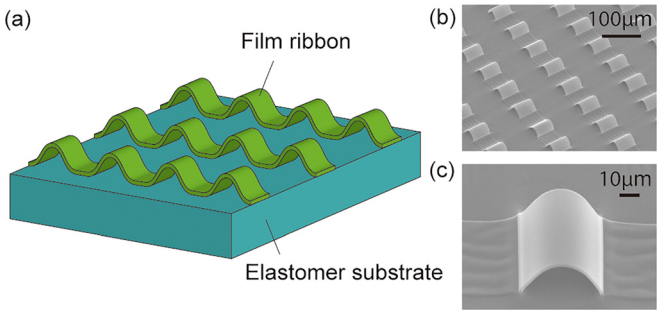

FIG. 1. (a) Schematic, (b) SEM image, and (c) magnified SEM image of the micro arch-bridge structure.

(Specialty Coating Systems Inc.), and polydimethylsiloxane (PDMS, Dow corning Corp.) for the thin ribbons and the elastomer substrate, respectively. A photoresist (S18-series, Tokyo Ohka Kogyo Co., Ltd.) was spin-coated at 3000 rpm for 30 s and patterned in fifty-micron-width ribbons by photolithography as shown in Figure 2(a1). The thickness of the resulting photoresist layer was 0.6 μm. On top of the patterned photoresist, a one-micron thick Parylene film with a Young's modulus 2.8 GPa (Ref. 21) was deposited on the entire surface of the elastomer substrate by CVD (Figure 2(a2)). Then, another photoresist layer was formed in fifty-micron line-and-space patterns perpendicular to the first photoresist pattern (Figure 2(a3)). The part of the Parylene thin film not covered by the photoresist was removed via the application of an oxygen plasma to form thin-film ribbons of Parylene. The first and second sets of the two photoresist ribbons were removed using acetone (Figure 2(a4)). The parts of the Parylene ribbons that had been in contact with the bare PDMS before the removal of the photoresist ribbons were strongly bonded to the bare PDMS (According to our previous work,[22,23] Parylene/PDMS bonding is maintained under stretch over 200% and compression over 40%). On the other hand, the parts of the Parylene ribbons that had been deposited on the photoresist ribbons before the removal of the photoresist ribbons were not bonded to the PDMS surface. By stretching the bilayer system in the direction perpendicular to the Parylene thin-film ribbons (in the y-direction), compression in the direction parallel to the ribbons (in the x-direction) was induced due to incompressibility of the substrate (Figure 2(a5)). Consequently, the Parylene ribbons buckled, and the micro arch-bridge structure shown in Figure 1 was achieved.

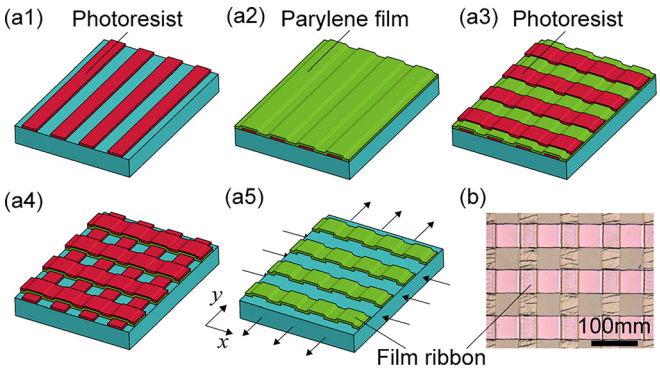

FIG. 2. (a) Fabrication steps for the micro arch-bridge structure. (b) Image of a fabricated bilayer system under no strain.

Figure 2(b) shows a photograph of the surface of the fabricated bilayer system under no strain. In this fabrication method, the thickness of the Parylene thin-film ribbons was 1 μm, while the thickness of the PDMS elastomer substrate was 300 μm. Therefore, we can assume that the PDMS elastomer substrate is infinitely thick for theoretical consideration. Although the Parylene thin film was patterned in the ribbon shape in the present case, the Parylene thin film and the bonded area can be patterned in various shapes by lithography: to show this potential, we made a thin-film table structure with the proposed method (Figure S1 in the supplementary material).

Experimental conditions are specified as follows: Under compression in the x-direction, the Parylene thin-film ribbons buckle, and the arch-bridge structure is formed. Experimentally, compressive strain in the x-direction was induced by stretch in the y-direction. Considering the volume conservation, the compressive strain ε is estimated as follows: The initial and current lengths in the x, y, and depth directions are denoted as L_x, L_y, L_z and L'_x, L'_y, L'_z, respectively. The compressive strain ε in the x-direction is given by $\varepsilon = 1 - L'_x/L_x$. Because of the volume conservation, $L'_x/L_x \times L'_y/L_y \times L'_z/L_z = 1$, and an (approximate) isotropic property, $L'_x/L_x = L'_z/L_z$, during the stretching, we estimate the compressive strain as $\varepsilon = 1 - (L'_y/L_y)^{-\frac{1}{2}}$. In the experiment, ε was estimated by measuring L'_y sequentially. The bilayer system was cut into a strip with dimensions L_x=10 mm and L_y=25 mm and stretched up to L'_y=45 mm (ε=0.25).

In Figure 3(a), we show the change in the geometry of the arch-bridge structure under increasing (forward transition) and decreasing (backward transition) compressive strain ε. The width (in the y-direction) of the Parylene ribbons is unchanged despite the stretch in the y-direction, whereas the width (in the y-direction) of the rows of the bare PDMS strips between the Parylene ribbons is strongly increased. This point may be understood by comparing, for example, Figures 3(a1) and 3(a4). The profile of the arch-bridge structure under various compressive strains ε was observed using an optical surface-measurement system consisting of a microscope and a laser profiler (VK-8710, Keyence Corp.).

Figure 3(a) shows the detail of the forward transition (compressive strain is increased). For a small compressive strain ($\varepsilon = 0.02$), the surface remains flat (Figure 3(a1)). Upon increasing compressive strain to $\varepsilon = 0.14$ (Figure 3(a2)), some unbonded regions form clear arch bridges, whereas the other unbonded regions remain almost flat (For $\varepsilon < 0.14$, clear arch bridges are not observed). Upon increasing compressive strain continuously to $\varepsilon = 0.20$, the number of clear arch bridges increases (Figure 3(a3)). At $\varepsilon = 0.25$, all the unbonded regions homogeneously buckle to form a regular array of arch bridges (Figure 3(a4)). We consider that the localized buckling at small deformations occurs not due to defects on the surface but to an energetic reason as explained in what follows. This inhomogeneous development of arch bridges is analogous to the one observed in a system in which a thin film attached to an elastomer substrate is delaminated from the elastomer substrate.[24,25] In Ref. 25, delamination of a thin film attached to the entire surface of

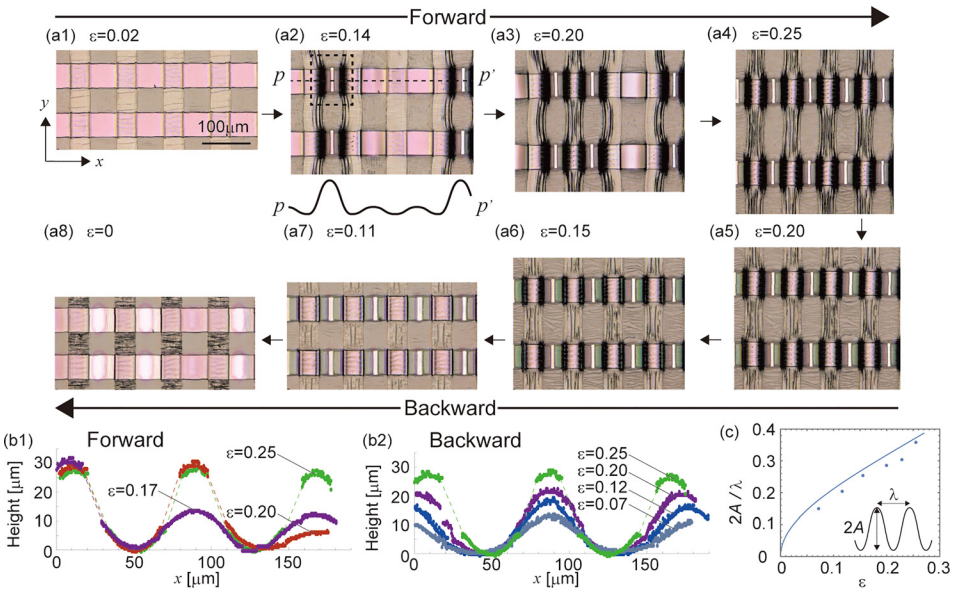

FIG. 3. (a) Surface morphology vs. compressive strain ε. (a1)–(a4) During the increase of ε, the arch bridges form inhomogeneously. (a5)–(a8) During the release of ε, the height of arch bridges decreases homogeneously. (b1) and (b2) Surface profiles of a ribbon during the increase and decrease of ε, respectively. Since parts of the profile with a steep slope cannot be measured with a laser profiler, missed parts are interpolated by dashed lines (the end points of obtained data are simply joined by straight dashed lines). (c) Aspect ratio $2A/\lambda$ vs. ε during the release. The solid line is the curve obtained from Eq. (1).

an elastomer substrate was studied through the experiment and numerical analysis. Even if defects are absent, the state in which the film is partially delaminated from the substrate can be energetically favorable compared with the state in which the film buckles homogeneously, when deformation is relatively small. As shown in Figures 3(a5)–3(a8), in contrast to the forward transition, the height of arch bridges decreases homogeneously with the decrease in ε.

Arch-bridges on a larger scale (one-hundred-micrometer scale) are presented in the supplementary material (Figure S2). In this case, the width of arch-bridges does not correspond to the width of the unbonded areas, and some irregular arch-bridges are observed. The formation of the irregular arch-bridges on a larger scale and a way to avoid the irregularity are explained in the supplementary material.

The profiles of the surface during the increase and decrease of ε are presented in Figures 3(b1) and 3(b2), respectively. Examination of the profiles shows that not only unbonded regions but also bonded regions are bent (unbonded regions detached from the substrate form arch bridges, whereas bonded regions are bent in the opposite direction).

The geometry of the arch-bridge structure during the decrease in ε can be explained theoretically in terms of the aspect ratio of the height $2A$ to the wavelength λ of the structure as demonstrated in Figure 3(c) that shows the relationship between $2A/\lambda$ and ε. Assuming that the profile has the form of $A + A\sin(2\pi x/\lambda)$, the ratio $2A/\lambda$ can be estimated by calculating the total length of the thin-film ribbon. The length of the ribbon under compression per period is given by $\frac{\lambda}{1-\varepsilon} = \int_0^{\lambda} dx\sqrt{1 + (2\pi A/\lambda)^2\cos^2(2\pi x/\lambda)}$. This expression, in the limit $A/\lambda \ll 1$, can be expressed as

$$2\frac{A}{\lambda} = \frac{2}{\pi}\left(\frac{\varepsilon}{1-\varepsilon}\right)^{\frac{1}{2}}. \quad (1)$$

This approximate expression is reasonably well confirmed in Figure 3(c). The maximum value $2\frac{A}{\lambda} = 0.36$ at $\varepsilon = 0.25$ is relatively high compared with other bilayer systems in which thin films are attached to the entire surface of elastomer substrates.[26]

We verified that the arch bridges are maintained and exhibit the same wetting property over repetitive placements of droplets (Figure 4(a)). This was shown through the measurement of the apparent contact angle at different ε. The bilayer system was stretched until $\varepsilon = 0.25$, and the compressive strain was then gradually released. During the release at a certain fixed ε, a droplet was placed on the surface, and the apparent contact angles were measured as a function of ε; at each ε, we newly placed a fresh droplet of the same volume on the same substrate by forming a droplet of 2 μl at the tip of the syringe needle via injection; the droplet was quasi-statically placed on the surface by slowly contacting it with the surface and deliberately separating it from the needle. At every ε, the droplet was placed three times, and the apparent contact angles were measured from the direction perpendicular (front view; see the inset of Figure 4(a)) and parallel (side view) to the thin-film ribbons. The measured apparent contact angles are plotted in Figure 4(a). At every ε, the

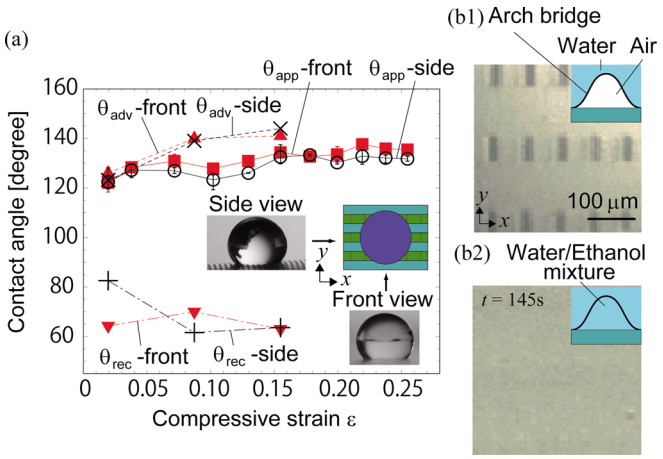

FIG. 4. (a) Contact angle on an arch-bridge structured surface as a function of ε. Photographs of a water droplet at $\varepsilon = 0.25$ from two different directions are embedded in the plot. Apparent (θ_{app}:■ and ○), advancing (θ_{adv}:▲ and ×), and receding (θ_{rec}:▼ and +) contact angles from the front and side views are shown in the plot. (b1) A water droplet placed on the surface. (b2) 145 s after ethanol is added to the water droplet (the amount is several times of the water-droplet volume).

difference between the maximum and minimum values is within 10 degrees (The top and bottom of the error bars correspond to the maximum and minimum values respectively, where the length of bars are smaller than the size of symbols in most cases). The differences in the observed angles at the same value of ε were small, which implies that the arch-bridge structure was not damaged after the repetitive placement of the droplet, maintaining the same wetting property. The robustness of the arch-bridge is also justified theoretically by considering the bending energy and the capillary energy[27] (for the details, see supplementary material in which the small shift in the contact angles with respect to ε is also discussed).

Additionally, we confirmed in Figure 4(a) that the contact angle hysteresis (CAH) is significantly large on the arch-bridge structure because of pinning effects. For the CAH measurement, the tip of the syringe was placed 2.3 mm above the surface, and the droplet was injected and withdrawn from the syringe with the droplet continuously in contact with the needle tip to observe the advancing and receding angles. The angles were observed from the front and side during the increase and decrease in the droplet volume (corresponding to the advancing and receding angles, respectively). As shown in Figure 4(a), the advancing and receding angles measured both from the front and side are 140° and 60°, respectively, at $\varepsilon = 0.15$, that is, CAH reaches 80°, whereas the value of the apparent contact angle is close to the advancing angle. We consider that the high CAH is caused by the pinning of the contact line at the edge of the structure and structured surfaces reported previously.[28,29]

In Figure 4(b), we further confirmed the robustness of the arch-bridge structure against the droplet deposition in a more direct manner by observing the arch-bridge structure at $\varepsilon = 0.25$ from below with a CCD camera. Figure 4(b1) shows the arch bridges which are in contact with a water droplet. The unbonded areas appear black, and this areas look black because air bubbles are trapped in the arch bridges (Due to the difference in the refractive index between liquid and air, the air bubbles are visible in the images). Figure 4(b2) shows the arch bridges 145 sec after adding ethanol to the water droplet. The liquid fully fills the hollow spaces, and the air bubbles disappear because the liquid invades the spaces beneath the arched ribbons (The significant difference may be caused by the difference in the wetting or the solvation property). We repeated the experiment illustrated in Figure 4(b2) and observed the same phenomena. Thus, we consider that the arch bridges are maintained in spite of repetitive deposition of droplets.

Finally, we present in Figure 5 that the surface exhibits the liquid-dependent iso/anisotropic wetting property (isotropic for water and anisotropic for ethanol). Figures 5(a)–5(e) show the difference in the profiles of a pure water droplet, water/ethanol (2:1, 1:1, and 1:2) mixture droplets, and a pure ethanol droplet observed from below, respectively, on the surface at $\varepsilon = 0.25$. The ratios of the width in the y-direction to that in the x-direction are in the range of 1.05 (pure water in Figure 5(a)) to 1.4 (pure ethanol in Figure 5(e)). The widths of the water droplet in the x- and y-directions are close to each other, whereas the width of the ethanol droplet in the y-direction is larger than that in the x-direction. The

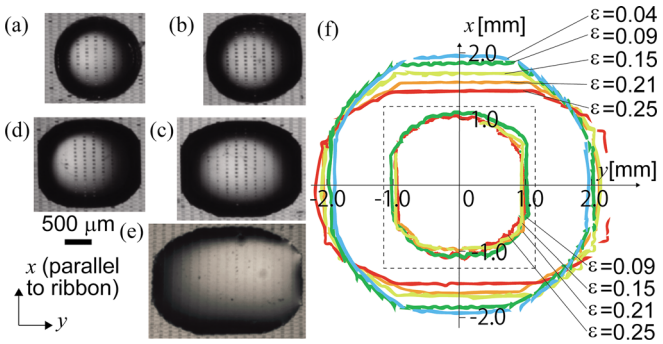

FIG. 5. Droplets of (a) pure water, (b)–(d) water/ethanol (2:1, 1:1, and 1:2) mixture, and (e) pure ethanol placed on the arch-bridge structure. (f) Change in the contact lines with ε of the water droplet (inside the dashed square) and an ethanol droplet (outside the dashed square) at a fixed volume of droplets (2 μl).

difference in the shapes originates from the difference in the state of arch-bridges: water cannot penetrate into the arch-bridge structure, whereas the ethanol/water mixture can (see Figure 4(b)). We expect that the arch-bridges promote the pinning of the contact line mentioned above and prevent the droplets from spreading in the direction parallel to the ribbons. This effect is common for water and ethanol droplets. On the other hand, in the direction perpendicular to the ribbons, the ethanol droplet can easily spread entering beneath the arch-bridges structure, whereas the water droplet cannot so that the width of the ethanol droplet in this direction is larger than that of the water droplet.

Furthermore, the degree of the anisotropy for ethanol is tunable by changing ε as shown in Figures 5(f), which gives the contact lines of the water and ethanol droplets, respectively, at different ε (Since the spherical surface of the water droplet is overhang due to the contact angle larger than 90 degrees, the profile in Figure 5(a) and the contact line in Figure 5(f) have different shapes). For ethanol, the width in the y-direction increases with ε, which makes the drop shape more anisotropic. This result demonstrates the tunability of the anisotropy in wetting on the surface. In contrast, for water, the widths of drops in the x- and y-directions are almost the same, and both widths do not change with ε.

This unique liquid-dependent iso/anisotropic wetting property is different from that of micro-machined structured surfaces of micro-pillars (e.g., cylinder post,[30] mushroom,[31,32] micro-hoodoo,[33,34] serif-T,[35,36] and micro-nail[37]). In fact, recently, various structures exhibiting anisotropic wetting properties both in Nature[38–40] and technology[1,28,41–44] have been studied. Our structure with hollow spaces induced by our kirigami-on-elastomer approach presents a way for achieving an unusual anisotropic wetting surface. Furthermore, in Nature, some creatures have structured surfaces composed of thin-film elements such as butterfly wings[38] and ligia exotica's legs,[45,46] and their surfaces exhibit anisotropic wetting and unusual imbibition properties, respectively. These functionalities are still hard to mimic due to difficulty in fabrication of such structures by the conventional micromachining. With our kirigami-on-elastomer approach, however, thin-film three-dimensional microstructures can be easily achieved. Thus, the present study provides a promising way for manufacturing thin-film functional surfaces.

In summary, the arch-bridge structure was achieved via the kirigami-on-elastomer approach. By using the CVD process, the transfer process became unnecessary, and thus, the present approach simplifies the previous method.[19,20] The morphology of the arch-bridge structure with respect to the compressive strain was studied experimentally with physical interpretations. The arch bridge is significantly robust and exhibits the liquid-dependent iso/anisotropic wetting property that can be controlled by ε. This paper presents a promising route for fabricating functional surfaces of thin-film/elastomer bilayer systems.

See supplementary material for the thin-film table structure and the arch bridge on a larger scale, and we discuss the small shift in the contact angles and the robustness of the arch bridge.

This research was partly supported by the ImPACT program of council for science, Technology and Innovation (Cabinet office government of Japan). This work was partially supported by a Grant-in-Aid for JSPS Fellows (Grant Nos. 16J00871 and 15J10394). We made the photomasks on the University of Tokyo VLSI Design and Education Center's (VDEC).

[1]J. Y. Chung, J. P. Youngblood, and C. M. Stafford, Soft Matter **3**, 1163–1169 (2007).
[2]P. C. Lin and S. Yang, Soft Matter **5**, 1011 (2009).
[3]S. G. Lee, D. Y. Lee, H. S. Lim, D. H. Lee, S. Lee, and K. Cho, Adv. Mater. **22**, 5013–5017 (2010).
[4]E. P. Chan and A. J. Crosby, Adv. Mater. **18**, 3238–3242 (2006).
[5]D. van den Ende, J.-D. Kamminga, A. Boersma, T. Andritsch, and P. G. Steeneken, Adv. Mater. **25**, 3438–3442 (2013).
[6]T. Ohzono, K. Suzuki, T. Yamaguchi, and N. Fukuda, Adv. Opt. Mater. **1**, 374–380 (2013).
[7]T. Xie, X. Xiao, J. Li, and R. Wang, Adv. Mater. **22**, 4390–4394 (2010).
[8]E. P. Chan and A. J. Crosby, Adv. Mater. **20**, 711 (2008).
[9]X. Jiang, S. Takayama, X. Qian, E. Ostuni, H. Wu, N. Bowden, P. LeDuc, D. E. Ingber, and G. M. Whitesides, Langmuir **18**, 3273–3280 (2002).
[10]M. Guvendiren and J. A. Burdick, Biomaterials **31**, 6511–6518 (2010).
[11]C. Cao, H. F. Chan, J. Zang, K. W. Leong, and X. Zhao, Adv. Mater. **26**, 1763–1770 (2014).
[12]F. Greco, T. Fujie, L. Ricotti, S. Taccola, B. Mazzolai, and V. Mattoli, Appl. Mater. Interfaces **5**, 573–584 (2013).
[13]M. R. Aufan, Y. Sumi, S. Kim, and J. Y. Lee, Appl. Mater. Interfaces **7**, 23454–23463 (2015).
[14]M. K. Blees, A. W. Barnard, P. A. Rose, S. P. Roberts, K. L. McGill, P. Y. Huang, A. R. Ruyack, J. W. Kevek, B. Kobrin, D. A. Muller, and P. L. McEuen, Nature **524**, 204 (2015).
[15]Z. Song, X. Wang, C. Lv, Y. An, M. Liang, T. Ma, D. He, Y. J. Zheng, S. Q. Huang, H. Yu, and H. Jiang, Sci. Rep. **5**, 10998 (2015).
[16]A. Lamoureux, K. Lee, M. Shlian, S. R. Forrest, and M. Shtein, Nat. Commun. **6**, 8092 (2015).
[17]T. Castle, Y. Cho, X. Gong, E. Jung, D. M. Sussman, S. Yang, and R. D. Kamien, Phys. Rev. Lett. **113**, 245502 (2014).
[18]M. Isobe and K. Okumura, Sci. Rep. **6**, 24758 (2016).
[19]Y. Zhang, Z. Yan, K. Nan, D. Xiao, Y. Liu, H. Luan, H. Fu, X. Wang, Q. Yang, J. Wang, W. Ren, H. Si, F. Liu, L. Yang, H. Li, J. Wang, X. Guo, H. Luo, L. Wang, Y. Huang, and J. A. Rogers, PNAS **112**, 11757–11764 (2015).
[20]S. Xu, Z. Yan, K. I. Jang, W. Huang, H. Fu, J. Kim, Z. Wei, M. Flavin, J. McCracken, R. Wang, A. Badea, Y. Liu, D. Xiao, G. Zhou, J. Lee, H. U. Chung, H. Cheng, W. Ren, A. Banks, X. Li, U. Paik, R. G. Nuzzo, Y. Huang, Y. Zhang, and J. A. Rogers, Science **347**, 154–159 (2015).
[21]See http://scscoatings.com for information about Parylene.
[22]A. Takei, L. Jin, J. W. Hutchinson, and H. Fujita, Adv. Mater. **26**, 4061–4067 (2014).
[23]A. Takei, L. Jin, and H. Fujita, ACS Appl. Mater. Interfaces **8**, 24230–24237 (2016).
[24]D. Vella, J. Bico, A. Boudaoud, B. Roman, and P. M. Reis, PNAS **106**, 10901–10906 (2009).
[25]Q. Wang and X. Zhao, J. Appl. Mech. **81**, 051004 (2014).
[26]Y. C. Chen and A. J. Crosby, Adv. Mater. **26**, 5626–5631 (2014).
[27]B. Roman and J. Bico, J. Phys.: Condens. Matter **22**, 493101 (2010).
[28]J. Bico, C. Marzolin, and D. Quere, Europhys. Lett **47**, 220–226 (1999).
[29]P. G. de Gennes, F. Brochard-Wyard, and D. Quéré, *Capillarity and Wetting Phenomena: Drops, Bubbles, Pearls, Waves* (Springer: New York, 2004).
[30]L. Courbin, E. Denieul, E. Dressaire, M. Roper, A. Ajdari, and H. A. Stone, Nat. Mater. **6**, 661–664 (2007).
[31]X. Chen, J. A. Weible, and S. V. Garimella, Sci. Rep. **5**, 17110 (2015).
[32]R. M. Nascimento, C. Cottin-Bizonne, C. Pirat, and S. M. M. Ramos, Langmuir **32**, 2005–2009 (2016).
[33]R. Dufour, M. Harnois, Y. Coffinier, V. Thomy, R. Boukherroub, and V. Senez, Langmuir **26**, 17242–17247 (2010).
[34]A. Tuteja, W. Choi, M. Ma, J. M. Mabry, S. A. Mazzella, G. C. Rutledge, G. H. McKinley, and R. E. Cohen, Science **318**, 1618–1622 (2007).
[35]R. Henzel, R. Helbig, S. Aland, H. G. Braun, A. Voigt, C. Neinhuis, and C. Werner, Langmuir **29**, 1100–1112 (2013).
[36]T. Liu and C. J. Kim, Science **346**, 1096–1100 (2014).
[37]A. Grigoryev, I. Tokarev, K. G. Kornev, I. Luzinov, and S. Minko, J. Am. Chem. Soc. **134**, 12916–12919 (2012).
[38]Y. Zheng, X. Gao, and L. Jiang, Soft Matter **3**, 178 (2007).
[39]H. Wu, R. Zhang, Y. Sun, D. Lin, Z. Sun, W. Pan, and P. Downs, Soft Matter **4**, 2429 (2008).
[40]S. G. Lee, H. S. Lim, D. Y. Lee, D. Kwak, and K. Cho, Adv. Funct. Mater. **23**, 547 (2013).
[41]Y. Zhao, Q. Lu, M. Li, and X. Li, Langmuir **23**, 6212–6217 (2007).
[42]D. Xia and S. R. J. Brueck, Nano Lett. **8**, 2819–2824 (2008).
[43]T. Kim and K. Y. Suh, Soft Matter **5**, 4131–4135 (2009).
[44]N. A. Malvadkar, M. J. Hancock, K. Sekeroglu, W. J. Dressick, and M. C. Demirel, Nat. Mater. **9**, 1023 (2010).
[45]D. Ishii, H. Horiguchi, Y. Hirai, H. Yabu, Y. Matsuo, K. Ijiro, T. Shimozawa, T. Hariyama, and M. Shimomura, Sci. Rep. **3**, 3024 (2013).
[46]M. Tani, D. Ishii, S. Ito, T. Hariyama, M. Shimomura, and K. Okumura, PLoS One **9**, e96813 (2014).